



One-Pot Hydrothermal Synthesis of MoS₂/Zn_{0.5}Cd_{0.5}S Heterojunction for Enhanced Photocatalytic H₂ Production

Xinru Li^{1,2}, Fei Xue³, Naixu Li⁴, Xukai Wei³, Hui Liu^{1*}, Jianchen Zhou⁴, Bin Lyu^{5,6} and Maochang Liu^{3*}

¹ School of Material Science and Engineering, Shaanxi University of Science and Technology, Xi'an, China, ² College of Petroleum Engineering, Xi'an Shiyou University, Xi'an, China, ³ International Research Center for Renewable Energy, State Key Laboratory of Multiphase Flow in Power Engineering, Xi'an Jiaotong University, Xi'an, China, ⁴ School of Chemistry and Chemical Engineering, Southeast University, Nanjing, China, ⁵ College of Bioresources Chemical and Materials Engineering, Shaanxi University of Science and Technology, Xi'an, China, ⁶ National Educational Reform Experimental Demonstration Center, Xi'an, China

OPEN ACCESS

Edited by:

Flavio Leandro De Souza,
Brazilian Nanotechnology National
Laboratory, Brazil

Reviewed by:

Guohong Wang,
Hubei Normal University, China
Konstantinos Christoforidis,
Democritus University of
Thrace, Greece

*Correspondence:

Hui Liu
liuhui@sust.edu.cn
Maochang Liu
maochangliu@mail.xjtu.edu.cn

Specialty section:

This article was submitted to
Catalysis and Photocatalysis,
a section of the journal
Frontiers in Chemistry

Received: 27 May 2020

Accepted: 24 July 2020

Published: 03 September 2020

Citation:

Li X, Xue F, Li N, Wei X, Liu H, Zhou J,
Lyu B and Liu M (2020) One-Pot
Hydrothermal Synthesis of
MoS₂/Zn_{0.5}Cd_{0.5}S Heterojunction for
Enhanced Photocatalytic H₂
Production. *Front. Chem.* 8:779.
doi: 10.3389/fchem.2020.00779

A series of molybdenum disulfide (MoS₂)/Zn_{0.5}Cd_{0.5}S heterojunctions have been prepared via a mild one-pot hydrothermal method based on the optimization of composition content of primary photocatalyst. The photocatalysts demonstrated significantly improved visible light-driven photocatalytic activity toward H₂ evolution from water without using any noble metal cocatalyst. Among the as-prepared composites, 0.2% MoS₂/Zn_{0.5}Cd_{0.5}S shows the best performance. The highest H₂ evolution rate reaches 21 mmol · g⁻¹ · h⁻¹, which is four times higher than that of pure Zn_{0.5}Cd_{0.5}S. The apparent quantum efficiency is about 46.3% at 425 nm. The superiority is attributed to the tight connection between MoS₂ and Zn_{0.5}Cd_{0.5}S by this facile one-step hydrothermal synthesis. As a result, the formation of the heterostructure introduces built-in electric field at the interface that facilitates vectorial charge transfer. More specifically, photogenerated electrons transfer to MoS₂ to conduct proton reduction, where the holes are retained on the surface of Zn_{0.5}Cd_{0.5}S to react with the sacrificial reagents. Moreover, the composite presents improved stability without notable activity decay after several cycled tests.

Keywords: photocatalysis, hydrogen production, sulfide, heterojunction, cocatalyst

INTRODUCTION

Derived from the high heat of combustion and carbon-neutral energy cycle, hydrogen energy has been envisaged as an appealing substitute for excessively depleted fossil resources (Kim et al., 2014). Since Fujishima and Honda (1972) as the pioneers discovered water photolysis on TiO₂ electrode in 1972, solar H₂ production on semiconductor-based photocatalysts has been widely accepted as an ideal strategy for addressing the imminent energy crisis and incremental pollution issues (Guo et al., 2018; Liu et al., 2018; Yang Y. et al., 2018; Jiao et al., 2020). The achievement of this technology lies in rational design and development of efficient and cost-effective photocatalysts with high quantum efficiency (Yan et al., 2009, 2011; Lin et al., 2017; Huckaba et al., 2018; Singh et al., 2018). Particularly, the visible light accounted for 43% of the whole solar spectrum (Guo et al., 2016). Therefore, in the past few decades, much effort has been attempted to synthesize visible light-driven

photocatalysts (Tan et al., 2016; Liu et al., 2017, 2018; Feng et al., 2018; Hafeez et al., 2018; Jin et al., 2018). Among the various photocatalysts, metal sulfides have been confirmed to be promising assignable to their superior photocatalytic performance (Tsuji et al., 2004; Iwashina et al., 2015; Di et al., 2016; Zhai et al., 2018). Specially, CdS is deemed as one of the most appropriate binary chalcogenide photocatalyst owing to the narrow band gap (~ 2.4 eV) for visible light response and the more negative conduction band position than reduction potential of H^+/H_2 (0 V vs. NHE, pH = 0) (Chao et al., 2017; Zhou et al., 2017; Yuan et al., 2018). Despite these inherent advantages of CdS photocatalyst, photocorrosion and toxicity should not be ignored. Motivated by well-matched coordination mode between CdS and ZnS, embedding Zn^{2+} into crystal cell of CdS to fabricated solid solution ($\text{Zn}_x\text{Cd}_{1-x}\text{S}$) has been found to increase the stability and photoactivity simultaneously (Liu et al., 2011, 2013; Yang M. et al., 2018).

To further boost the photoactivity of $\text{Zn}_x\text{Cd}_{1-x}\text{S}$ photocatalysts, integrating suitable cocatalysts to trap charges carriers and serve as delicate surface reactive sites would be a productive approach. However, as the most common cocatalyst, the application of noble metals (e.g., Pt and Pd) can be confined only to bench scale because of their high cost and scarcity (Gao et al., 2019; Li et al., 2020a,b). Therefore, the exploration and development of alternative noble metal-free but active cocatalysts are highly desired. Up to now, plenty of earth-abundant transition metal compounds are developed as efficient and non-precious cocatalysts (Zong et al., 2008; Akple et al., 2015; He et al., 2017; Zhang et al., 2017, 2018; Xu et al., 2018). Among them, molybdenum disulfide (MoS_2) with layered structures has attracted wide attention because of optimized surface binding free energy of H atoms, large layered structure determined surface area, and excellent structural adjustability (Frame et al., 2010; Li et al., 2013; Qi et al., 2013; Chung et al., 2014; He et al., 2016; Zeng et al., 2017). Furthermore, some other works disclosed the superior cocatalytic function of MoS_2 over TiO_2 , g- C_3N_4 , and CdS, indicating its general applicability (Zhou et al., 2012; Parayil et al., 2013; Chai et al., 2018; Zhang et al., 2018). It is highly noted that the assembly of MoS_2 and primary photocatalysts is usually achieved by the time-consuming two-step method, bringing about a weak interfacial interaction for charge transfer and inferior stability (Zong et al., 2008; Frame et al., 2010; Zhou et al., 2012; He et al., 2016). In contrast, one-pot hydrothermal approach has been certified to be feasible to fabricate tight connected interface between photocatalyst and cocatalyst. It can be thus expected that MoS_2 could integrate on the $\text{Zn}_x\text{Cd}_{1-x}\text{S}$ surface with enhanced physicochemical property.

Herein, we reported a simple and low-cost one-step hydrothermal method for coating MoS_2 onto the surface of $\text{Zn}_x\text{Cd}_{1-x}\text{S}$ directly. The series of photocatalysts with different weight ratio between MoS_2 and $\text{Zn}_x\text{Cd}_{1-x}\text{S}$ exhibited superior photocatalytic performance toward H_2 evolution within $\text{Na}_2\text{S}/\text{Na}_2\text{SO}_3$ aqueous solution. When the capacity of MoS_2 is 0.2%, the highest activity was approached, with an H_2 production rate of $21 \text{ mmol} \cdot \text{h}^{-1} \cdot \text{g}^{-1}$. Moreover, the durability was further improved by the incorporation of MoS_2 . The improvement dominantly depends on the smooth transfer of electrons through

the intimate interface induced by the one-pot hydrothermal route and promoted surface redox reaction at the numerously increased active sites. It is believed that this work could inspire the application of other noble metal-free cocatalyst decorated photocatalyst with highly efficient photocatalytic activity.

EXPERIMENTAL SECTION

Chemicals and Materials

Cadmium acetate [$\text{Cd}(\text{CH}_3\text{COO})_2 \cdot 2\text{H}_2\text{O}$], zinc acetate [$\text{Zn}(\text{CH}_3\text{COO})_2 \cdot 2\text{H}_2\text{O}$], thioacetamide (TAA, $\text{C}_2\text{H}_5\text{NS}$), sodium molybdate ($\text{Na}_2\text{MoO}_4 \cdot 2\text{H}_2\text{O}$), sodium sulfide ($\text{Na}_2\text{S} \cdot 9\text{H}_2\text{O}$), sodium sulfite (Na_2SO_3), and ethanol ($\text{CH}_3\text{CH}_2\text{OH}$) were used as received. The water used in all syntheses was deionized (DI) water with a resistivity of $18.2 \text{ M}\Omega \cdot \text{cm}$.

One-Pot Hydrothermal Synthesis of $\text{Zn}_x\text{Cd}_{1-x}\text{S}$ Solid Solution

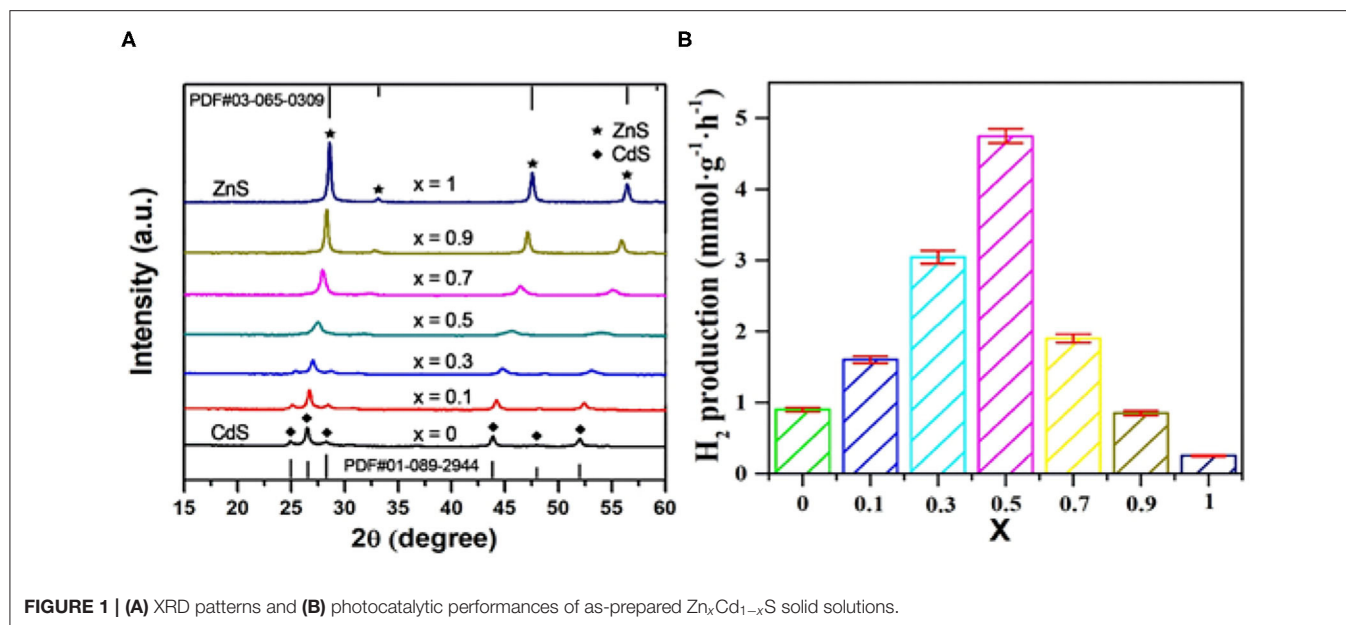
TAA 50 mmol was first dissolved into 35 mL ethanol. Then the ethanol solution was mixed with 35 mL aqueous solution containing certain amount of $\text{Cd}(\text{CH}_3\text{COO})_2 \cdot 2\text{H}_2\text{O}$ and $\text{Zn}(\text{CH}_3\text{COO})_2 \cdot 2\text{H}_2\text{O}$ (the total mole number of Cd and Zn precursor is 20 mmol). After stirring for 20 min at 800 revolutions/min (rpm), the suspension was transferred to the 100 mL Teflon-lined stainless steel autoclave, followed by heat treatment at 200°C for 48 h. Based on cooling down naturally, the obtained product was centrifuged and washed with ethanol and deionized water for several times. A yellow powder is prepared by drying the product under vacuum at 80°C for 5 h. Finally, prepared samples were labeled as $\text{Zn}_x\text{Cd}_{1-x}\text{S}$, where x equals 0, 0.1, 0.3, 0.5, 0.7, 0.9, and 1, respectively, indicating the stoichiometric ratio between Zn and S.

One-Pot Hydrothermal Synthesis of $\text{MoS}_2/\text{Zn}_{0.5}\text{Cd}_{0.5}\text{S}$ Nanocomposites

Ethanol 35 mL and TAA 50 mmol were dissolved into a 35 mL aqueous solution containing 10 mmol $\text{Cd}(\text{CH}_3\text{COO})_2 \cdot 2\text{H}_2\text{O}$ and 10 mmol $\text{Zn}(\text{CH}_3\text{COO})_2 \cdot 2\text{H}_2\text{O}$. Then 5 mL aqueous solution containing a certain amount $\text{Na}_2\text{MoO}_4 \cdot 2\text{H}_2\text{O}$ (0; 0.002; 0.004; 0.006 mmol) was added to it with continuous stirring at 800 rpm. After that, the mixture was transferred to a 100 mL Teflon-lined autoclave and heated at 200°C for 48 h. After cooling down to room temperature, the resultant product was obtained by centrifugation and washed with deionized water and ethanol for several times thoroughly. Then it was dried at 80°C in a vacuum oven. According to the difference of concentrations of MoS_2 , the final $\text{MoS}_2/\text{Zn}_{0.5}\text{Cd}_{0.5}\text{S}$ was designed as $\text{Zn}_{0.5}\text{Cd}_{0.5}\text{S}$, 0.1% $\text{MoS}_2/\text{Zn}_{0.5}\text{Cd}_{0.5}\text{S}$, 0.2% $\text{MoS}_2/\text{Zn}_{0.5}\text{Cd}_{0.5}\text{S}$, and 0.3% $\text{MoS}_2/\text{Zn}_{0.5}\text{Cd}_{0.5}\text{S}$, respectively.

Photocatalytic Reactions

The photocatalytic performance of various photocatalysts from the same batch was estimated one after another. Photocatalytic reactions of hydrogen production from water were conducted in a gas-closed system with a side irradiation Pyrex cell (using PLS-SXE300/300UV Xe lamp irradiation) at 35°C . The



photocatalyst powder was dispersed by a magnetic stirrer in an aqueous solution (180 mL) containing Na_2S (0.35 M) and Na_2SO_3 (0.25 M) as electron donors. After being evacuated by N_2 gas with a heavy flow for over 20 min, the photocatalysts were irradiated with visible light ($\lambda \geq 430$ nm) through a cutoff filter from the Xe lamp. The intensity and number of photons of the light source were measured by a fiber-optic spectrometer. The amount of H_2 gas was determined using online gas chromatography (NaX zeolite column, TCD detector, N_2 carrier) or drainage at every hour interval. Blank experiments showed that no H_2 was produced. Apparent quantum yield (AQY) defined by Equation (1) was measured using a 425-nm band-pass filter and an irradiate meter.

$$AQY = \frac{\text{the number of reacted electrons}}{\text{the number of incident photons}} = \frac{\text{the number of evolved } H_2 \text{ molecules} \times 2}{\text{the number of incident photons}} \quad (1)$$

(Photo)electrochemical Measurements

A CHI760d electrochemical workstation (Chenhua Instruments Co., Shanghai, China) was applied to record transient photocurrent response, electrochemical impedance spectra (EIS), and Mott-Schottky (MS) plot. In a typical (photo)electrochemical test, a standard three-electrode system with the sample as working electrode, Ag/AgCl (in saturated KCl) as reference electrode, Pt wire as counter electrode, and sodium sulfate aqueous solution (0.5 M) as the electrolyte was employed. An Xe lamp with a simulated solar light filter (AM 1.5) was adopted as the light source for transient photocurrent response tests. For the preparation of working electrodes, 1 mg of as-synthesized samples and 20 μ L of 5% Nafion (DuPont) were uniformly dispersed in 1 mL of water-ethanol mixture solution. After ultrasonication treatment to the mixture for 1 h, 0.5 mL of homogeneous suspension was dropped onto a 2 \times

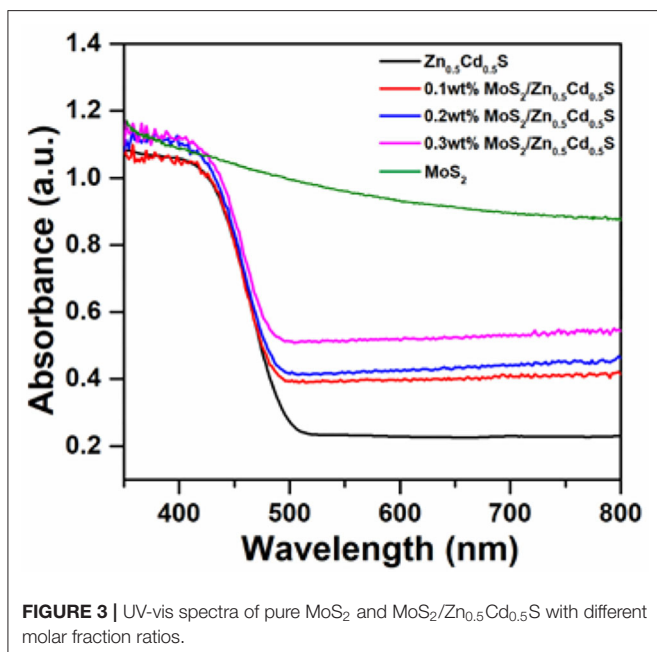
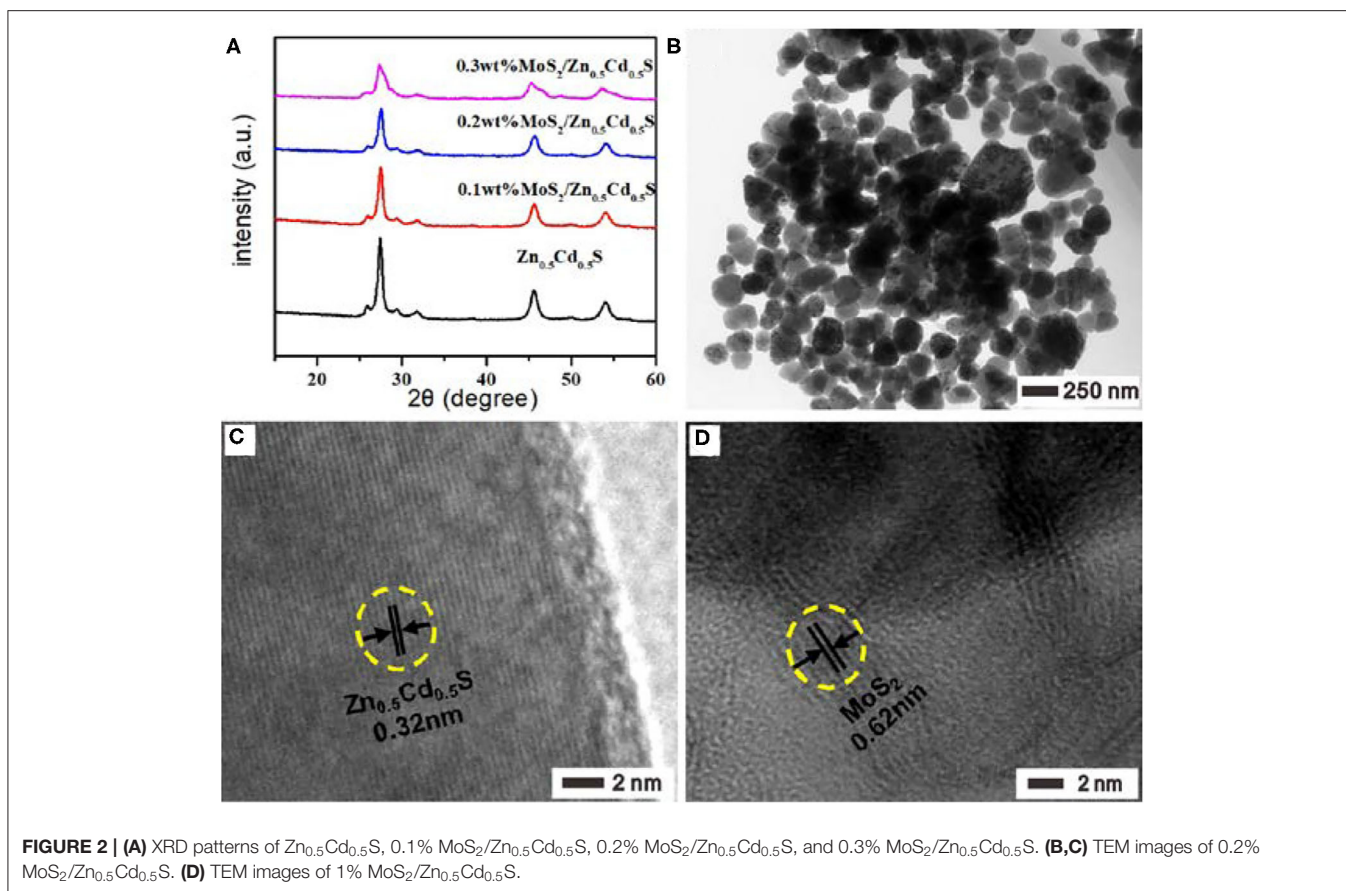
3-cm fluorine-doped tin oxide glass plate. When the samples were naturally dried under ambient temperature, the working electrodes could be obtained.

Characterizations

X-ray diffraction (XRD) patterns of prepared photocatalysts were confirmed by an X'Pert PRO diffractometer using $Cu K\alpha$ ($\lambda = 0.1538$ nm) irradiation with constant instrument parameter. Diffuse reflectance ultraviolet-visible (UV-vis) spectra were measured on a Hitachi U-4100 spectrometer, equipped with a lab-sphere diffuse reflectance accessory. The crystallite morphologic micrographs were observed by JEOL JSM-7800F field emission scanning electron microscopy and FEI Tecnai G2 F30 transmission electron microscope (TEM). The X-ray photoelectron spectroscopy (XPS) measurements were conducted on Axis Ultra, Kratos (UK) multifunctional spectrometer using monochromatic Al $K\alpha$ radiation. The C 1s peak at 284.8 eV of adventitious carbon was used for calibration.

RESULTS AND DISCUSSION

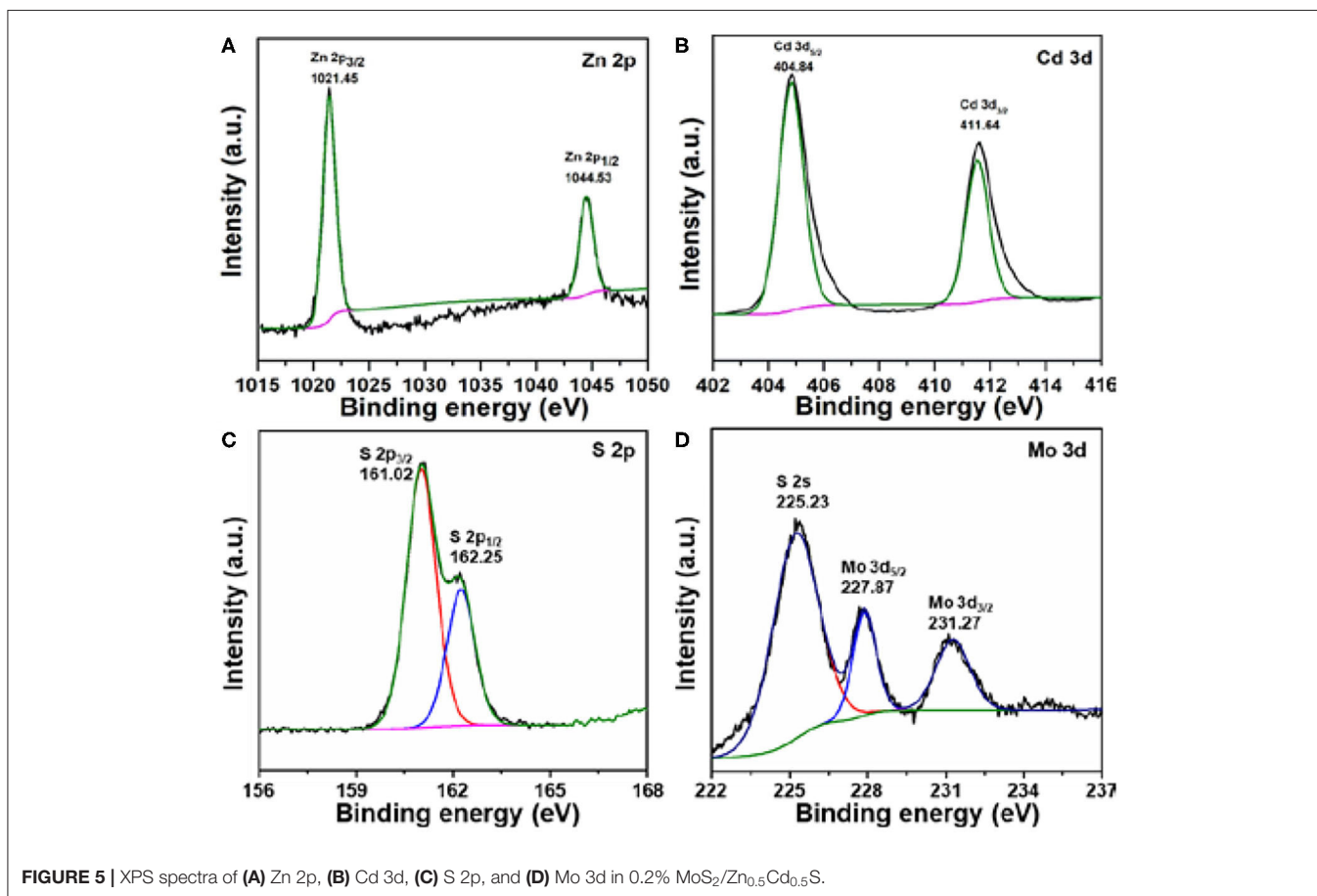
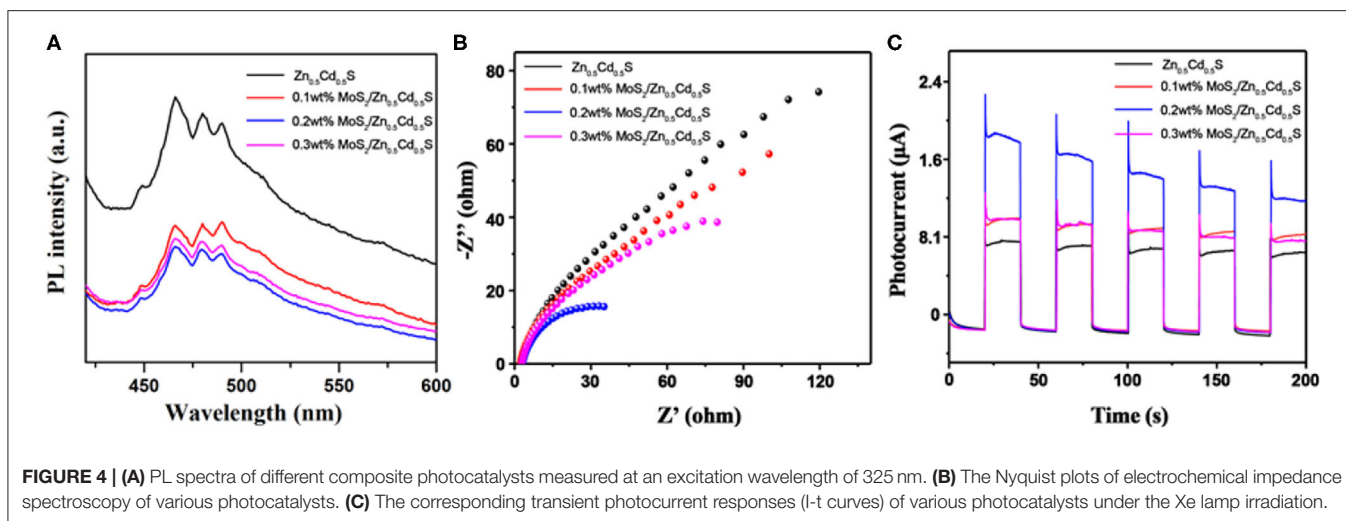
The prepared composites were first investigated by XRD. As shown in **Figure 1A**, comparing with the standard XRD patterns (JCPDS 03-065-0309 for zinc-blende ZnS, JCPDS 01-089-2944 for wurtzite-type CdS), the x -value-dependent phase transition from wurtzite-type structure ($x < 0.5$) to zinc-blended structure ($x \geq 0.5$) was definitely observed. Likewise, on the premise of the same phase structure, all the $Zn_xCd_{1-x}S$ samples manifested a successive and systematical diffraction peak shift to higher angle with the increase of x -value, implying the successful formation of solid solution (Yang M. et al., 2018). Photocatalytic tests toward H_2 evolution over these $Zn_xCd_{1-x}S$ photocatalysts behaved a significant volcano trend along with the change of x value (**Figure 1B**). When the Zn/Cd ratio reached 1:1, $Zn_{0.5}Cd_{0.5}S$



exhibited the highest activity with an H_2 evolution rate of $4.5 \text{ mmol} \cdot \text{g}^{-1} \cdot \text{h}^{-1}$. In principle, the continuous incorporation

of Zn^{2+} into CdS lattice is expected to sequentially broaden the band gap of the solution. On the one hand, the wider band gap signifies the narrow light absorption range; on the other hand, it also forebodes the enhanced reduction potential of electrons that resulted from the upshifted conduction band position. Therefore, it is of great benefit for improving photocatalytic activity by coordinating the balance between these two contradictions. As a circumstance, $Zn_{0.5}Cd_{0.5}S$ with the suitable band gap and relatively negative conduction band position showed the superior photoactivity in our case. In subsequent investigation, $Zn_{0.5}Cd_{0.5}S$ was taken as the primary photocatalyst to integrate with MoS_2 for construction of composites.

The MoS_2 with various loading amounts were then introduced onto the surface of $Zn_{0.5}Cd_{0.5}S$ via the facile one-pot hydrothermal method. To gain insight into the microstructures, the as-prepared $MoS_2/Zn_{0.5}Cd_{0.5}S$ samples were first characterized by XRD. As observed in **Figure 2A**, all the samples were found with identical diffraction peak positions regardless of the MoS_2 loading amount, indicating the crystal structure of $Zn_{0.5}Cd_{0.5}S$ was independent of MoS_2 . Further observation revealed the obviously decreased diffraction intensity at 27.6° with the increase of MoS_2 introduction, which should be ascribed to the scattering and absorption effect of MoS_2 to the incident X-ray. This notion also verified the tight connection between these two



components indirectly, offering a great opportunity to improve the catalytic properties (Zhang et al., 2019). In contrast, no visible diffraction peaks could be discerned to MoS₂ because of its small amount exceeding detection limit. The surface morphology and particle sizes, taking 0.2% MoS₂/Zn_{0.5}Cd_{0.5}S as a model photocatalysts, were tested by high-resolution

(HR) TEM. In **Figure 2B**, the uniformly dispersed composite particles showed a size of ~120 nm. The HRTEM image of 0.2% MoS₂/Zn_{0.5}Cd_{0.5}S sample in **Figure 2C** demonstrated the construction of Zn_{0.5}Cd_{0.5}S solid solution again. Specifically, the smooth fringes of ~0.32 nm can be indexed to the (111) plane diffraction of Zn_{0.5}Cd_{0.5}S (Liu et al., 2011). Unfortunately,

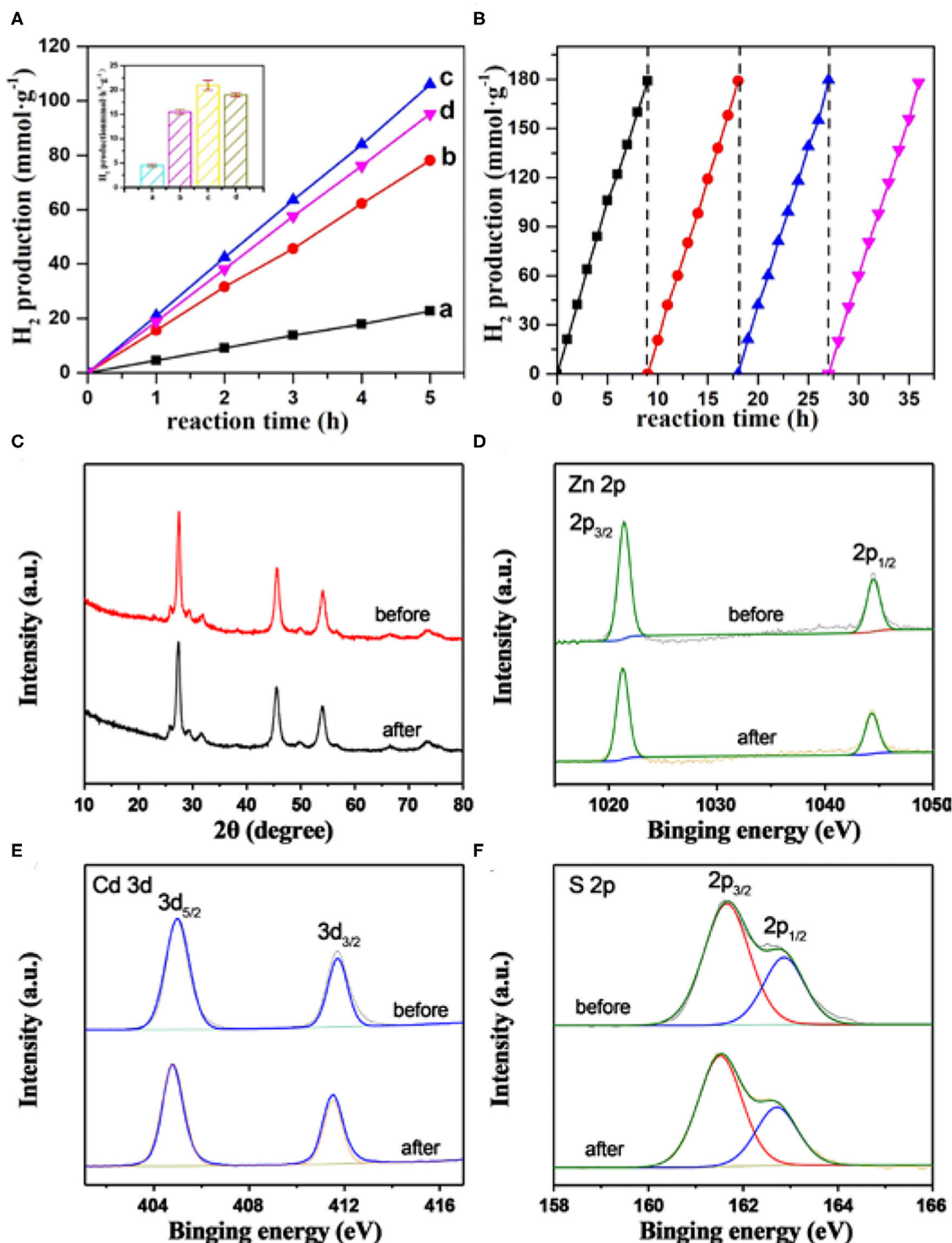


FIGURE 6 | (A) Time-coursed photocatalytic H₂ evolution activity of MoS₂/Zn_{0.5}Cd_{0.5}S composites with various MoS₂ content in aqueous solution containing 0.25M Na₂S and 0.35M Na₂SO₃. Herein, (a) Zn_{0.5}Cd_{0.5}S, (b) 0.1% MoS₂/Zn_{0.5}Cd_{0.5}S, (c) 0.2% MoS₂/Zn_{0.5}Cd_{0.5}S, (d) 0.3% MoS₂/Zn_{0.5}Cd_{0.5}S. **(B)** Time courses of recycling tests toward photocatalytic H₂ evolution over 0.2% MoS₂/Zn_{0.5}Cd_{0.5}S composite photocatalyst. **(C)** XRD patterns and XPS spectra of **(D)** Zn 2p, **(E)** Cd 3d, **(F)** S 2p in 0.2% MoS₂/Zn_{0.5}Cd_{0.5}S before and after 3-time recycling tests. The inset in **(A)** is the photocatalytic H₂ evolution rate of MoS₂/Zn_{0.5}Cd_{0.5}S composites with various MoS₂ content.

it is almost impossible to observe the lattice fringes of MoS₂ owing to the low mass ratio of MoS₂. To this end, the TEM image of 1% MoS₂/Zn_{0.5}Cd_{0.5}S with a larger MoS₂ content instead was analyzed by HRTEM, as shown in **Figure 2D**. In this case, the lattice spacing of 0.62 nm corresponding to the (002) planes of MoS₂ can be clearly noticed (Zong et al., 2008), ensuring the successful coating of MoS₂ on the surface of Zn_{0.5}Cd_{0.5}S. At the same time, it also testified the intimate tangency at atomic scale between MoS₂ and Zn_{0.5}Cd_{0.5}S. In principle, this unique heterojunction structure should facilitate photogenerated charges separation and migration at the atomic scale (Zong et al., 2008; Akple et al., 2015; He et al., 2017).

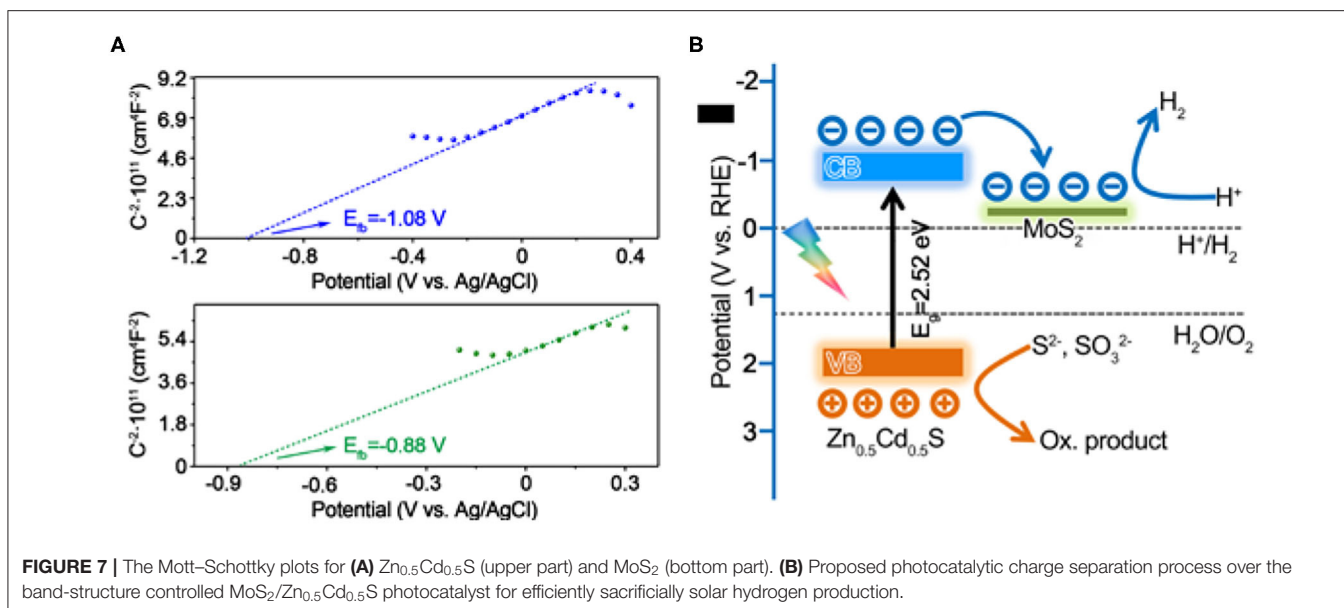
To uncover the optical property of as-prepared composites, some crucial characterizations were then carried out. The UV-vis absorption spectra of MoS₂/Zn_{0.5}Cd_{0.5}S samples are presented in **Figure 3**. The pure Zn_{0.5}Cd_{0.5}S nanocrystal exhibited an apparent absorption band edge at ~492 nm. The band gap of Zn_{0.5}Cd_{0.5}S thus can be estimated to be 2.52 eV, respectively. Furthermore, pristine MoS₂ exhibited a strong light absorbance in the whole UV and visible region. The notion implies the metallic property of MoS₂, foreboding a high potential to be cocatalyst. For the MoS₂/Zn_{0.5}Cd_{0.5}S composites, they showed no distinct difference in absorption band. Nonetheless, the light absorption at longer wavelength between 520 and 800 nm was obviously increased. This enhancement was gradually amplified with the increased content of MoS₂. All the phenomena above collectively confirm that the inherent band structure of Zn_{0.5}Cd_{0.5}S is well-preserved even after coupling MoS₂, indicating that MoS₂ was merely adhered on the surface of Zn_{0.5}Cd_{0.5}S tightly rather than Mo⁴⁺ incorporated into the Zn_{0.5}Cd_{0.5}S crystal lattice.

Subsequently, the composite photocatalysts were investigated by PL. The spectra with an excitation wavelength of 325 nm are displayed in **Figure 4**. Pure Zn_{0.5}Cd_{0.5}S exhibited a strong intrinsic emission peak, indicating severe recombination of free carriers in Zn_{0.5}Cd_{0.5}S. As MoS₂ was integrated with Zn_{0.5}Cd_{0.5}S, a similar spectrum trend with significantly quenched PL intensity of composites was observed, confirming the crucial function of MoS₂ in accelerating the charge carriers transfer (Wang et al., 2019, 2020a,b). The optimized photogenerated carriers' dynamics also can be concluded from some other photoelectrochemical characterizations, including electrochemical impedance spectroscopy (EIS) and transient photocurrent response. As exhibited in **Figure 4B**, the smaller radius on the Nyquist plots of composites than that of pure Zn_{0.5}Cd_{0.5}S verifies the dramatically promoted electronic conductivity from Zn_{0.5}Cd_{0.5}S to MoS₂ (Wang et al., 2019, 2020a,b). Meanwhile, the smallest semicircle of 0.2% MoS₂/Zn_{0.5}Cd_{0.5}S certifies the content superiority. **Figure 4C** shows the transient photocurrent responses of samples in chopped illumination cycles. The enhanced photocurrent response of composite indicates the significant role of MoS₂ in accelerating charge separation and improving surface reaction kinetics (Wang et al., 2019, 2020a,b). Notably, a small content of MoS₂ (i.e., 0.1% MoS₂/Zn_{0.5}Cd_{0.5}S) could induce insufficient active sites in the catalyst, whereas a large

amount of MoS₂ (i.e., 0.3% MoS₂/Zn_{0.5}Cd_{0.5}S) would introduce new recombination centers. Both situations are unfavorable to depress the recombination rate of carriers and thus with limited ability to boost the redox reaction. As a result, 0.2% MoS₂/Zn_{0.5}Cd_{0.5}S with the lowest PL signal, smallest EIS radius, and highest photocurrent could be expected to have a higher photocatalytic performance (Bi et al., 2016).

We next sought to understand the surface chemical states by using XPS analysis. Taking 0.2% MoS₂/Zn_{0.5}Cd_{0.5}S as an example, the XPS survey scans shown in **Figure 5** revealed the existence of all the expected elements. The tiny peak intensity of Mo certified the low content in composite. The HR Zn 2p XPS spectra displayed two peaks at binding energies of 1,021.45 and 1,044.53 eV, which can be assigned to Zn 2p_{3/2} and Zn 2p_{1/2}, respectively (**Figure 5A**; Qin et al., 2017). Meanwhile, the two well-defined peaks centered at 404.84 and 411.64 eV in the HR Cd 3d XPS spectra represented Cd 3d_{5/2} and Cd 3d_{3/2}, respectively (**Figure 5B**). For sulfur, it was demonstrated in the chemical state of S²⁻ (**Figure 5C**). The above analysis provided further proofs on the formation of Zn_{0.5}Cd_{0.5}S solid solution. Furthermore, the peaks of Mo 3d appearing at binding energies of 227.87 and 231.27 eV belong to Mo 3d_{5/2} and Mo 3d_{3/2}, respectively. It indicates that Mo⁴⁺ is the dominant chemical state (**Figure 5D**). More importantly, these peaks solidly indicate the 1T phase for MoS₂ in 0.2% MoS₂/Zn_{0.5}Cd_{0.5}S (2H at 229.0 and 232.3 eV) (Wang et al., 2013). Generally, MoS₂ with 1T phase can function as a cocatalyst because of its metallic character (Bai et al., 2015). These results evidently confirm the successful synthesis of MoS₂ cocatalyst (He et al., 2016; Zhang et al., 2018). Collectively, the XPS analysis further confirmed the coexistence of MoS₂ and Zn_{0.5}Cd_{0.5}S solid solution in composites.

The photocatalytic activity toward H₂ production from water over the MoS₂/Zn_{0.5}Cd_{0.5}S composite photocatalysts was then evaluated under visible-light irradiation (**Figure 6A**). No H₂ evolution was detected without either illumination or photocatalyst, indicating the photocatalytic function of MoS₂/Zn_{0.5}Cd_{0.5}S composite photocatalysts. As displayed in **Figure 6A**, the photocatalytic hydrogen production via water splitting increased linearly with time. Pure Zn_{0.5}Cd_{0.5}S showed a low photocatalytic activity due to the rapid recombination of electron-hole pairs. While the introduction of the MoS₂ cocatalyst gave rise to a significant improvement in the photocatalytic H₂ evolution, this phenomenon can be explained by the fact that MoS₂ can effectively extract electron from Zn_{0.5}Cd_{0.5}S and act as the active site of photocatalytic H₂ production. More importantly, an MoS₂ content-dependent volcano-type trend for the activity was also acquired. With a low content of MoS₂, although the charge transfer dynamics can be accelerated in some degree, the insufficient active sites restrict the extraction of electrons from Zn_{0.5}Cd_{0.5}S and the surface reaction rates. However, too much MoS₂ introduction will impede optical absorption, shield the photoactive sites, and induce new recombination centers. Therefore, the hydrogen production rate was reduced in the two cases. With the optimal loading amount of cocatalyst, 0.2% MoS₂/Zn_{0.5}Cd_{0.5}S showed the highest hydrogen production rate of 21 mmol · h⁻¹ · g⁻¹, deriving from the appropriate photoabsorption,



charge transfer rate, and active sites. The activity is four times higher than that of $\text{Zn}_{0.5}\text{Cd}_{0.5}\text{S}$. Meanwhile, the AQY of 0.2% $\text{MoS}_2/\text{Zn}_{0.5}\text{Cd}_{0.5}\text{S}$ was also measured to be as high as 46.3% at 425 nm. The photostability of the composite photocatalysts was also evaluated by taking 0.2% $\text{MoS}_2/\text{Zn}_{0.5}\text{Cd}_{0.5}\text{S}$ as an example. As seen from **Figure 6B**, continuous hydrogen output with constant rate over 0.2% $\text{MoS}_2/\text{Zn}_{0.5}\text{Cd}_{0.5}\text{S}$ was clearly appreciable, even if this reaction proceeded for more than 30 h. The above result enunciates the desirable chemical stability of the as-prepared composite photocatalysts. Moreover, the XRD (**Figure 6C**) and XPS (**Figures 6D–F**) examination of the 0.2% $\text{MoS}_2/\text{Zn}_{0.5}\text{Cd}_{0.5}\text{S}$ after a three-time recycling test, without unveiling non-detectable alternations relative to fresh sample, provided further evidence for the sufficient protection of MoS_2 to the primary $\text{Zn}_{0.5}\text{Cd}_{0.5}\text{S}$ photocatalyst.

In order to acquire the photocatalytic mechanism of the composite, the band alignment should be determined first. The exact band level can be determined by an intercept method in MS plots together with the band gap derived from the UV-vis absorbance spectra. As exhibited in **Figure 7A**, the flat band potentials (E_{fb}) of $\text{Zn}_{0.5}\text{Cd}_{0.5}\text{S}$ and MoS_2 were estimated to be -0.47 and -0.27 V (vs. RHE), respectively. Generally, the CB position is considered to be more negative by 0.2 eV than E_{fb} for semiconductor. Accordingly, the authentic CB for $\text{Zn}_{0.5}\text{Cd}_{0.5}\text{S}$ is -0.67 V (vs. RHE). Combining the band gap of $\text{Zn}_{0.5}\text{Cd}_{0.5}\text{S}$ that was determined to be 2.52 eV, the VB of $\text{Zn}_{0.5}\text{Cd}_{0.5}\text{S}$ is calculated to be 1.85 V (vs. RHE), respectively, while for the metallic MoS_2 , the flat band potentials approximately equal its Fermi level (E_f) (Ran et al., 2017). Based on the above analysis, the photocatalytic pathway over $\text{MoS}_2/\text{Zn}_{0.5}\text{Cd}_{0.5}\text{S}$ composite photocatalysts was illustrated in **Figure 7B**. From a thermodynamic viewpoint, both E_g and E_{CB} of $\text{Zn}_{0.5}\text{Cd}_{0.5}\text{S}$ satisfy the precondition for photocatalytic H_2 generation. Hence, this reaction process under assistant of $\text{Zn}_{0.5}\text{Cd}_{0.5}\text{S}$ would take place very smoothly. Upon exposing to visible light, the electrons in VB of $\text{Zn}_{0.5}\text{Cd}_{0.5}\text{S}$

will be excited to its CB to induce electron-hole pairs. Because of the thermodynamic driving force induced by the distance between low Fermi level of MoS_2 and high CB of $\text{Zn}_{0.5}\text{Cd}_{0.5}\text{S}$, together with the small interface barriers that stemmed from strong interaction between MoS_2 and $\text{Zn}_{0.5}\text{Cd}_{0.5}\text{S}$ caused by one-pot hydrothermal treatment, the electrons on $\text{Zn}_{0.5}\text{Cd}_{0.5}\text{S}$ will directionally migrate to MoS_2 , leading to a spatial separation of these charge carriers (Chang et al., 2015; Yin et al., 2016). As a result, the protons will be effectively reduced to be H_2 at active sites provided by MoS_2 , accompanied by transfer of holes to surface of $\text{Zn}_{0.5}\text{Cd}_{0.5}\text{S}$ for consumption by the sacrificial agents, leading to the promotion of photocatalytic activity over these $\text{MoS}_2/\text{Zn}_{0.5}\text{Cd}_{0.5}\text{S}$ composites.

CONCLUSIONS

In summary, a series of $\text{MoS}_2/\text{Zn}_{0.5}\text{Cd}_{0.5}\text{S}$ composite photocatalysts have been successfully constructed. The success relies upon a mild one-pot hydrothermal process for incorporating MoS_2 on the surface of $\text{Zn}_{0.5}\text{Cd}_{0.5}\text{S}$ solid solution in identical growth environment. All the composite photocatalysts showed significant enhancement in solar hydrogen evolution. The highest photoactivity was achieved over the 0.2% $\text{MoS}_2/\text{Zn}_{0.5}\text{Cd}_{0.5}\text{S}$ photocatalyst, with an H_2 production rate of $21 \text{ mmol} \cdot \text{h}^{-1} \cdot \text{g}^{-1}$ and an AQY of 46.3% at 425 nm, highlighting the intense promoting effect of MoS_2 as a cocatalyst. Specifically, MoS_2 can steer the electrons through the interface between these two components by strong interfacial interaction formed in a one-pot hydrothermal method. Meanwhile, abundant active sites provided by MoS_2 also can facilitate the surface redox reaction. This work provides the feasibility to develop noble metal-free cocatalyst incorporating a photocatalyst system for efficient and stable H_2 evolution.

DATA AVAILABILITY STATEMENT

All datasets presented in this study are included in the article/supplementary material.

AUTHOR CONTRIBUTIONS

XL and FX: conceptualization, methodology, formal analysis, writing—original draft, visualization, and data curation. NL: methodology, formal analysis, and data curation. XW: experimental assistant. HL: writing—review and editing, and project administration. JZ and BL: result discussion. ML: conceptualization, methodology, writing—review and editing,

supervision, project administration, and funding acquisition. All authors contributed to the article and approved the submitted version.

FUNDING

This work was supported by the National Nature Science Foundation of China (No. 51876173), the Natural Science Foundation of Jiangsu Province (No. BK20190054), the China Fundamental Research Funds for the Central Universities, and the Shaanxi Technical Innovation Guidance Project (No. 2018HJCG-14).

REFERENCES

- Akple, M. S., Low, J., Wageh, S., Al-Ghamdi, A. A., Yu, J., Zhang, J., et al. (2015). Enhanced visible light photocatalytic H₂-production of g-C₃N₄/WS₂ composite heterostructures. *Appl. Surf. Sci.* 358, 196–203. doi: 10.1016/j.apsusc.2015.08.250
- Bai, S., Wang, L., Chen, X., Du, J., and Xiong, Y. (2015). Chemically exfoliated metallic MoS₂ nanosheets: a promising supporting co-catalyst for enhancing the photocatalytic performance of TiO₂ nanocrystals. *Nano Res.* 8, 175–183. doi: 10.1007/s12274-014-0606-9
- Bi, L., Meng, D., Bu, Q., Lin, Y., Wang, D., and Xie, T. (2016). Electron acceptor of Ni decorated porous carbon nitride applied in photocatalytic hydrogen production. *Phys. Chem. Chem. Phys.* 18, 31534–31541. doi: 10.1039/C6CP05618K
- Chai, B., Xu, M., Yan, J., and Ren, Z. (2018). Remarkably enhanced photocatalytic hydrogen evolution over MoS₂ nanosheets loaded on uniform CdS nanospheres. *Appl. Surf. Sci.* 430, 523–530. doi: 10.1016/j.apsusc.2017.07.292
- Chang, K., Li, M., Wang, T., Ouyang, S., Li, P., Liu, L., et al. (2015). Drastic layer-number-dependent activity enhancement in photocatalytic H₂ evolution over n MoS₂/CdS (n≥1) under visible light. *Adv. Energy Mater.* 5:1402279 doi: 10.1002/aenm.201402279
- Chao, Y., Zheng, J., Chen, J., Wang, Z., Jia, S., Zhang, H., et al. (2017). Highly efficient visible light-driven hydrogen production of precious metal-free hybrid photocatalyst: CdS@NiMoS core-shell nanorods. *Catal. Sci. Technol.* 7, 2798–2804. doi: 10.1039/C7CY00964J
- Chung, D. Y., Park, S. K., Chung, Y. H., Yu, S. H., Lim, D. H., Jung, N., et al. (2014). Edge-exposed MoS₂ nano-assembled structures as efficient electrocatalysts for hydrogen evolution reaction. *Nanoscale* 6, 2131–2136. doi: 10.1039/C3NR05228A
- Di, T., Zhu, B., Zhang, J., Cheng, B., and Yu, J. (2016). Enhanced photocatalytic H₂ production on CdS nanorod using cobalt-phosphate as oxidation cocatalyst. *Appl. Surf. Sci.* 389, 775–782. doi: 10.1016/j.apsusc.2016.08.002
- Feng, J., Cheng, L., Zhang, J., Okoth, O. K., and Chen, F. (2018). Preparation of BiVO₄/ZnO composite film with enhanced visible-light photoelectrocatalytic activity. *Ceram. Int.* 44, 3672–3677. doi: 10.1016/j.ceramint.2017.11.124
- Frame, F. A., and F. E., Osterloh (2010). CdSe-MoS₂: a quantum size-confined photocatalyst for hydrogen evolution from water under visible light. *J. Phys. Chem. C* 114, 10628–10633. doi: 10.1021/jp101308e
- Fujishima, A., and Honda, K. (1972). Electrochemical photolysis of water at a semiconductor electrode. *Nature* 238, 37–38. doi: 10.1038/238037a0
- Gao, L., Li, X., Yao, Z., Bai, H., Lu, Y., Ma, C., et al. (2019). Unconventional p-d hybridization interaction in PtGa ultrathin nanowires boosts oxygen reduction electrocatalysis. *J. Am. Chem. Soc.* 141, 18083–18090. doi: 10.1021/jacs.9b07238
- Guo, L., Yang, Z., Marcus, K., Li, Z., Luo, B., Zhou, L., et al. (2018). MoS₂/TiO₂ heterostructures as nonmetal plasmonic photocatalysts for highly efficient hydrogen evolution. *Energy Environ. Sci.* 11, 106–114. doi: 10.1039/C7EE02464A
- Guo, S., Min, Y., Fan, J., and Xu, Q. (2016). Stabilizing and improving solar H₂ generation from Zn_{0.5}Cd_{0.5}S nanorods@MoS₂/RGO hybrids via dual charge transfer pathway. *ACS Appl. Mater. Interfaces* 8, 2928–2934. doi: 10.1021/acsami.5b06009
- Hafeez, H. Y., Lakhera, S. K., Bellamkonda, S., Rao, R., Shankar, M. V., Bahnemann, D. W., et al. (2018). Construction of ternary hybrid layered reduced graphene oxide supported g-C₃N₄-TiO₂ nanocomposite and its photocatalytic hydrogen production activity. *Int. J. Hydrog. Energy* 43, 3892–3904. doi: 10.1016/j.ijhydene.2017.09.048
- He, J., Chen, L., Wang, F., Liu, Y., Chen, P., Au, C. T., et al. (2016). CdS nanowires decorated with ultrathin MoS₂ nanosheets as an efficient photocatalyst for hydrogen evolution. *ChemSuschem* 9, 624–630. doi: 10.1002/cssc.201501544
- He, K., Xie, J., Yang, Z., Shen, R., Fang, Y., Ma, S., et al. (2017). Earth-abundant WC nanoparticles as an active noble-metal-free Co-catalyst for the highly boosted photocatalytic H₂ production over g-C₃N₄ nanosheets under visible light. *Catal. Sci. Technol.* 7, 1193–1202. doi: 10.1039/C7CY00029D
- Huckaba, A. J., Shirley, H., Lamb, R. W., Guertin, S., Autry, S., Cheema, H., et al. (2018). A mononuclear tungsten photocatalyst for H₂ production. *ACS Catal.* 8, 4838–4847. doi: 10.1021/acscatal.7b04242
- Iwashina, K., Iwase, A., Ng, Y. H., Amal, R., and Kudo, A. (2015). Z-schematic water splitting into H₂ and O₂ using metal sulfide as a hydrogen-evolving photocatalyst and reduced graphene oxide as a solid-state electron mediator. *J. Am. Chem. Soc.* 137, 604–607. doi: 10.1021/ja511615s
- Jiao, S., Fu, X., Zhang, L., Zeng, Y. J., and Huang, H. (2020). Point-defect-optimized electron distribution for enhanced electrocatalysis: towards the perfection of the imperfections. *Nano Today* 30:100833. doi: 10.1016/j.nantod.2019.100833
- Jin, Y. J., Linghu, J., Chai, J., Chua, C. S., Wong, L. M., Feng, Y. P., et al. (2018). Defect evolution enhanced visible-light photocatalytic activity in nitrogen-doped anatase TiO₂ thin films. *J. Phys. Chem. C* 122, 16600–16606. doi: 10.1021/acs.jpcc.8b04517
- Kim, H. J., Lee, S. H., Upadhye, A. A., Ro, I., Tegedor-Tegedor, I., Anderson, M. A., et al. (2014). Plasmon-enhanced photoelectrochemical water splitting with size-controllable gold nanodot arrays. *ACS Nano* 8, 10756–10765. doi: 10.1021/nn504484u
- Li, X., Ge, Z., Xue, F., Liu, H., Lyu, B., and Liu, M. (2020a). Lattice-oriented contact in Pd/SrTiO₃ heterojunction for rapid electron transfer during photocatalytic H₂ production. *Mater. Res. Bull.* 123:110722. doi: 10.1016/j.materresbull.2019.110722
- Li, X., Li, X., Liu, C., Huang, H., Gao, P., Ahmad, F., et al. (2020b). Atomic-level construction of tensile-strained PdFe alloy surface toward highly efficient oxygen reduction electrocatalysis. *Nano Lett.* 20, 1403–1409. doi: 10.1021/acs.nanolett.9b05024
- Li, Y., Li, Y. L., Araujo, C. M., Luo, W., and Ahuja, R. (2013). Single-layer MoS₂ as an efficient photocatalyst. *Catal. Sci. Technol.* 3, 2214–2220. doi: 10.1039/c3cy00207a
- Lin, H., Li, Y., Li, H., and Wang, X. (2017). Multi-node CdS hetero-nanowires grown with defect-rich oxygen-doped MoS₂ ultrathin nanosheets for efficient visible-light photocatalytic H₂ evolution. *Nano Res.* 10, 1377–1392. doi: 10.1007/s12274-017-1497-3
- Liu, J., Jia, Q., Long, J., Wang, X., Gao, Z., Gu, Q., et al. (2018). Amorphous NiO as co-catalyst for enhanced visible-light-driven hydrogen

- generation over g-C₃N₄ photocatalyst. *Appl. Catal. B Environ.* 222, 35–43. doi: 10.1016/j.apcatb.2017.09.073
- Liu, M., Jing, D., Zhou, Z., and Guo, L. (2013). Twin-induced one-dimensional homojunctions yield high quantum efficiency for solar hydrogen generation. *Nat. Commun.* 4:2278. doi: 10.1038/ncomms3278
- Liu, M., Wang, L., Lu, G., Yao, X., and Guo, L. (2011). Twins in Cd_{1-x}Zn_xS solid solution: highly efficient photocatalyst for hydrogen generation from water. *Energy Environ. Sci.* 4, 1372–1378. doi: 10.1039/c0ee00604a
- Liu, Y., Liu, S., Wu, T., Lin, H., and Zhang, X. (2017). Facile preparation of flower-like Bi₂WO₆/CdS heterostructured photocatalyst with enhanced visible-light-driven photocatalytic activity for Cr(VI) reduction. *J. Sol Gel Sci. Technol.* 83, 315–323. doi: 10.1007/s10971-017-4416-x
- Parayil, S. K., Baltrusaitis, J., Wu, C. M., and Koodali, R. T. (2013). Synthesis and characterization of ligand stabilized CdS-trititanate composite materials for visible light-induced photocatalytic water splitting. *Int. J. Hydrog. Energy* 38, 2656–2669. doi: 10.1016/j.ijhydene.2012.12.042
- Qi, Z., Cao, P., and Park, H. S. (2013). Density functional theory calculation of edge stresses in monolayer MoS₂. *J. Appl. Phys.* 114:163508. doi: 10.1063/1.4826905
- Qin, Z., Xue, F., Chen, Y., Shen, S., and Guo, L. (2017). Spatial charge separation of one-dimensional Ni₂P-Cd_{0.9}Zn_{0.1}S/g-C₃N₄ heterostructure for high-quantum-yield photocatalytic hydrogen production. *Appl. Catal. B Environ.* 217, 551–559. doi: 10.1016/j.apcatb.2017.06.018
- Ran, J., Zhu, B., and Qiao, S. Z. (2017). Phosphorene co-catalyst advancing highly efficient visible-light photocatalytic hydrogen production. *Angew. Chem. Int. Ed.* 56, 10373–10377. doi: 10.1002/anie.201703827
- Singh, R., and S., Dutta (2018). A review on H₂ production through photocatalytic reactions using TiO₂/TiO₂-assisted catalysts. *Fuel* 220, 607–620. doi: 10.1016/j.fuel.2018.02.068
- Tan, T. H., Scott, J., Ng, Y. H., Taylor, R. A., Aguey-Zinsou, K., and Amal, R. (2016). Understanding plasmon and band gap photoexcitation effects on the thermal-catalytic oxidation of ethanol by TiO₂-supported gold. *ACS Catal.* 6, 1870–1879. doi: 10.1021/acscatal.5b02785
- Tsuji, I., Kato, H., Kobayashi, H., and Kudo, A. (2004). Photocatalytic H₂ evolution reaction from aqueous solutions over band structure-controlled (AgIn)_xZn_{2(1-x)}S₂ solid solution photocatalysts with visible-light response and their surface nanostructures. *J. Am. Chem. Soc.* 126, 13406–13413. doi: 10.1021/ja048296m
- Wang, H., Lu, Z., Xu, S., Kong, D., Cha, J. J., Zheng, G., et al. (2013). Electrochemical tuning of vertically aligned MoS₂ nanofilms and its application in improving hydrogen evolution reaction. *Proc. Natl. Acad. Sci. U.S.A.* 110, 19701–19706. doi: 10.1073/pnas.1316792110
- Wang, J., Wang, G., Cheng, B., Yu, J., and Fan, J. (2020a). Sulfur-doped g-C₃N₄/TiO₂ S-scheme heterojunction photocatalyst for Congo Red photodegradation. *Chin. J. Catal.* 42, 56–68. doi: 10.1016/S1872-2067(20)63634-8
- Wang, J., Wang, G., Jiang, J., Wan, Z., Su, Y., and Tang, H. (2020b). Insight into charge carrier separation and solar-light utilization: rGO decorated 3D ZnO hollow microspheres for enhanced photocatalytic hydrogen evolution. *J. Coll. Interface Sci.* 564, 322–332. doi: 10.1016/j.jcis.2019.12.111
- Wang, J., Wang, G., Wang, X., Wu, Y., Su, Y., and Tang, H. (2019). 3D/2D direct Z-scheme heterojunctions of hierarchical TiO₂ microflowers/g-C₃N₄ nanosheets with enhanced charge carrier separation for photocatalytic H₂ evolution. *Carbon* 149, 618–626. doi: 10.1016/j.carbon.2019.04.088
- Xu, D., Xu, P., Zhu, Y., Peng, W., Li, Y., Zhang, G., et al. (2018). High yield exfoliation of WS₂ crystals into 1-2 layer semiconducting nanosheets and efficient photocatalytic hydrogen evolution from WS₂/CdS nanorod composites. *ACS Appl. Mater. Interfaces* 10, 2810–2818. doi: 10.1021/acsmi.7b15614
- Yan, H., and H., Yang (2011). TiO₂-g-C₃N₄ composite materials for photocatalytic H₂ evolution under visible light irradiation. *J. Alloys Comp.* 509, L26–L29. doi: 10.1016/j.jallcom.2010.09.201
- Yan, H., Yang, J., Ma, G., Wu, G., Zong, X., Lei, Z., et al. (2009). Visible-light-driven hydrogen production with extremely high quantum efficiency on Pt-PdS/CdS photocatalyst. *J. Catal.* 266, 165–168. doi: 10.1016/j.jcat.2009.06.024
- Yang, M., Wang, Y., Ren, Y., Liu, E., Fan, J., and Hu, X. (2018). Zn/Cd ratio-dependent synthetic conditions in ternary ZnCdS quantum dots. *J. Alloys Comp.* 752, 260–266. doi: 10.1016/j.jallcom.2018.04.084
- Yang, Y., Yin, L., Gong, Y., Niu, P., Wang, J., Gu, L., et al. (2018). An Unusual strong visible-light absorption band in red anatase TiO₂ photocatalyst induced by atomic hydrogen-occupied oxygen vacancies. *Adv. Mater.* 30:1704479. doi: 10.1002/adma.201704479
- Yin, X., Li, L., Jiang, W., Zhang, Y., Zhang, X., Wan, L., et al. (2016). MoS₂/CdS nanosheets-on-nanorod heterostructure for highly efficient photocatalytic H₂ generation under visible light irradiation. *ACS Appl. Mater. Interfaces* 8, 15258–15266. doi: 10.1021/acsami.6b02687
- Yuan, Y. J., Li, Z., Wu, S., Chen, D., Yang, L. X., Cao, D., et al. (2018). Role of two-dimensional nanointerfaces in enhancing the photocatalytic performance of 2D-2D MoS₂/CdS photocatalysts for H₂ production. *Chem. Eng. J.* 350, 335–343. doi: 10.1016/j.cej.2018.05.172
- Zeng, S., Zhang, L., Wang, W., Shao, D., and Hao, H. (2017). Hydrogen evolution based on the electrons/protons stored on amorphous TiO₂. *Phys. Chem. Chem. Phys.* 19, 29053–29056. doi: 10.1039/C7CP06067J
- Zhai, H., Liu, X., Huang, B., and Zhang, Q. f. (2018). Enhanced photocatalytic H₂ production of Mn_{0.5}Cd_{0.5}S solid solution through loading transition metal sulfides XS (X=Mo, Cu, Pd) cocatalysts. *Appl. Surf. Sci.* 430, 515–522. doi: 10.1016/j.apsusc.2017.08.056
- Zhang, G., Lan, Z. A., and Wang, X. (2017). Surface engineering of graphitic carbon nitride polymers with cocatalysts for photocatalytic overall water splitting. *Chem. Sci.* 8, 5261–5274. doi: 10.1039/C7SC01747B
- Zhang, Y., Peng, Z., Guan, S., and Fu, X. (2018). Novel β-NiS film modified CdS nanoflowers heterostructure nanocomposite: extraordinarily highly efficient photocatalysts for hydrogen evolution. *Appl. Catal. B Environ.* 224, 1000–1008. doi: 10.1016/j.apcatb.2017.11.043
- Zhang, Z., Ahmad, F., Zhao, W., Yan, W., Zhang, W., Huang, H., et al. (2019). Enhanced electrocatalytic reduction of CO₂ via chemical coupling between indium oxide and reduced graphene oxide. *Nano Lett.* 19, 4029–4034. doi: 10.1021/acs.nanolett.9b01393
- Zhou, F. Q., Fan, J. C., Xu, Q. J., and Min, Y. L. (2017). BiVO₄ nanowires decorated with CdS nanoparticles as Z-scheme photocatalyst with enhanced H₂ generation. *Appl. Catal. B Environ.* 201, 77–83. doi: 10.1016/j.apcatb.2016.08.027
- Zhou, W., Yin, Z., Du, Y., Huang, X., Zeng, Z., Fan, Z., et al. (2012). Synthesis of few-layer MoS₂ nanosheet-coated TiO₂ nanobelt heterostructures for enhanced photocatalytic activities. *Small* 9, 140–147. doi: 10.1002/smll.201201161
- Zong, X., Yan, H., Wu, G., Ma, G., Wen, F., Wang, L., et al. (2008). Enhancement of photocatalytic H₂ evolution on CdS by loading MoS₂ as cocatalyst under visible light irradiation. *J. Am. Chem. Soc.* 130, 7176–7177. doi: 10.1021/ja8007825

Conflict of Interest: The authors declare that the research was conducted in the absence of any commercial or financial relationships that could be construed as a potential conflict of interest.

Copyright © 2020 Li, Xue, Li, Wei, Liu, Zhou, Lyu and Liu. This is an open-access article distributed under the terms of the Creative Commons Attribution License (CC BY). The use, distribution or reproduction in other forums is permitted, provided the original author(s) and the copyright owner(s) are credited and that the original publication in this journal is cited, in accordance with accepted academic practice. No use, distribution or reproduction is permitted which does not comply with these terms.